Transsynaptic Teneurin Signaling in Neuromuscular Synapse Organization and Target Choice

Timothy J. Mosca[*], **Weizhe Hong**[*], **Vardhan S. Dani**, **Vincenzo Favaloro**, and **Liqun Luo**
Department of Biology, Howard Hughes Medical Institute, Stanford University, Stanford, CA 94305

Abstract

Synapse assembly requires transsynaptic signals between the pre- and postsynapse[1], but the understanding of essential organizational molecules remains incomplete[2]. Teneurins are conserved, EGF-repeat containing transmembrane proteins with large extracellular domains[3]. Here we show that two *Drosophila* Teneurins, Ten-m and Ten-a, are required for neuromuscular synapse organization and target selection. Ten-a is presynaptic while Ten-m is mostly postsynaptic; neuronal Ten-a and muscle Ten-m form a complex *in vivo*. Pre- or postsynaptic Teneurin perturbations cause severe synapse loss and impair many facets of organization transsynaptically and cell-autonomously. These include defects in active zone apposition, release sites, membrane and vesicle organization, and synaptic transmission. Moreover, the presynaptic microtubule and postsynaptic spectrin cytoskeletons are severely disrupted, suggesting a mechanism whereby Teneurins organize the cytoskeleton, which in turn affects other aspects of synapse development. Supporting this, Ten-m physically interacts with α-spectrin. Genetic analyses of *teneurin* and *neuroligin* reveal their differential roles that synergize to promote synapse assembly. Finally, at elevated endogenous levels, Ten-m regulates specific motoneuron-muscle target selection. Our study identifies the Teneurins as a key bi-directional transsynaptic signal in general synapse organization, and demonstrates that such a molecule can also regulate target selection.

Vertebrate Teneurins are enriched in the developing brain[4,5], localized to synapses in culture[6] and pattern visual connections[7]. Both *Drosophila* Teneurins, Ten-m and Ten-a, function in olfactory synaptic partner matching[8] and were further identified in neuromuscular junction (NMJ) defect screens[9,10], with Ten-m also affecting motor axon guidance[11]. We examine here their roles and underlying mechanisms in synapse development.

Both Teneurins were enriched at the larval NMJ (Fig. 1a, S1a). Ten-a was detected at neuronal membranes: this staining was undetectable beyond background in *ten-a* null mutants (Fig. S1b) and barely detectable following neuronal *ten-a* RNAi (Fig. S1c), indicating that Ten-a is predominantly presynaptic. Partial colocalization was observed between Ten-a and the periactive zone marker Fasciclin II[12] as well as the active zone marker Bruchpilot[13] (Fig. 1b–c), suggesting a localization between these regions. Ten-m appeared strongly postsynaptic and surrounded each bouton (Fig. 1a, S1a, d). Muscle-specific *ten-m* RNAi eliminated the postsynaptic staining, but uncovered weak presynaptic staining (Fig. S1e) that ubiquitous *ten-m* RNAi eliminated (Fig. S1f). Thus, the Ten-m signal was specific and, while partly presynaptic, enriched postsynaptically. Consistently, muscle Ten-m colocalized extensively with Dlg (Fig. 1d) and completely with α-spectrin (Fig. 1e) and is thus, likely coincident with all postsynaptic membranes.

The localization of Ten-a and Ten-m suggested their transsynaptic interaction. To examine this, we co-expressed myc-tagged Ten-a in nerves using the Q system[14] and HA-tagged Ten-m in muscles using GAL4. Muscle Ten-m was able to co-immunoprecipitate nerve Ten-a from larval synaptosomes (Fig. 1f), suggesting that the Teneurins form a heterophilic transsynaptic receptor pair at the NMJ.

To determine Teneurin function at the NMJ, we examined the *ten-a* null allele and larvae with neuron or muscle RNAi of *ten-a* and/or *ten-m*. Following such perturbations, bouton number and size were altered: the quantity was reduced by 55% (Fig 2a–c, g, S2) and the incidence of large boutons markedly increased (Fig. S2k). Both elements represent impaired synaptic morphogenesis. The reduction in bouton number was likely cumulative through development, as it was visible in first instar *ten-a* mutants and persisted (Fig. S2k). In the *ten-a* mutant, bouton morphogenesis was rescued by restoring Ten-a expression in neurons, but not muscles (Fig. 2d,g, S2). Neuronal Ten-m overexpression could not substitute for the lack of Ten-a, revealing their nonequivalence (Fig. S2e,l). Neuronal knockdown of Ten-a or Ten-m both showed an impairment (Fig. S2f–h,l), indicating presynaptic function for both, though presynaptic Ten-a plays a more significant role (Fig. S2l). Moreover, knocking down postsynaptic Ten-m in the *ten-a* mutant did not enhance the phenotype (Fig. 2g). Thus, presynaptic Ten-a (and to a lesser extent, Ten-m) and postsynaptic Ten-m are required for synapse development.

Perturbation of *teneurins* also caused defects in the apposition between presynaptic active zones (release sites) and postsynaptic glutamate receptor clusters[15] (Fig. 2h, S3): up to 15% of the active zones/receptor clusters lacked their partner compared to 1.8% in controls (Fig. 2h–k). Under electron microscopy, active zones are marked by electron dense membranes and single presynaptic specializations called T-bars (Fig. 2l), which enable synapse assembly, vesicle release and Ca^{2+} channel clustering[16]. Teneurin disruption caused defects (Fig. 2m-r, S3) in T-bar ultrastructure (Fig. 2m–o), membrane organization and apposition to contractile tissue (Fig. 2p–q). Teneurin perturbation also impaired postsynaptic densities while increasing membrane ruffling (Table S1), further indicating organizational impairment. These phenotypes resemble mutants with adhesion and T-bar biogenesis defects[17,18], suggesting a role for Teneurins in synaptic adhesion and stability. Synaptic vesicle populations similarly required Teneurins for clustering at the bouton perimeter and

proper density (Fig. S4). As these effects are not synonymous with active zone disruption[19], Teneurins are also required for synaptic vesicle organization.

Synapses lacking *teneurin* were also functionally impaired. The mean amplitude of evoked excitatory postsynaptic potentials (EPSP) in larvae was decreased by 28% in the *ten-a* mutant (Fig. 2s, u). Spontaneous miniature EPSPs (mEPSPs) showed a 20% decrease in amplitude, a 46% decrease in frequency (Fig. 2t, u) and an altered amplitude distribution compared with control (Fig. S5a). These defects resulted in a 20% reduction in quantal content (Fig. 2u), which could be partly due to fewer boutons and release sites. However, release probability may also be reduced, as suggested by an increased paired pulse ratio in *ten-a* mutants (Fig. S5d,e). The decay kinetics of responses were faster in *ten-a* mutants, suggesting additional postsynaptic effects on glutamate receptors and/or intrinsic membrane properties (Fig. S5b–c). Further, FM1-43 dye loading revealed markedly defective vesicle cycling in *ten-a* mutants (Fig. S5f–h). Consistent with physiological impairment, *teneurin*-perturbed larvae exhibited profound locomotor defects (Fig. S5i). In summary, Teneurins are required for multiple aspects of NMJ organization and function.

As a potential mechanism for synaptic disorganization following *teneurin* perturbation, we examined the pre- and postsynaptic cytoskeletons. In the presynaptic terminal, organized microtubules contain Futsch (a microtubule-binding protein)-positive "loops" while disorganized microtubules possess punctate, "unbundled" Futsch[20]. Each classification normally represented ~10% (often distal) of boutons (Fig. 3a, d, S6). Following *teneurin* perturbation, many more boutons had unbundled Futsch (Fig. 3b–c, S6) while those with looped microtubules were decreased by 62–95% (Fig. 3d). Therefore, proper microtubule organization requires pre- and postsynaptic Teneurins. In contrast to mild active zone/glutamate receptor apposition defects, most boutons displayed microtubule organizational defects.

Removal of *teneurins* also severely disrupted the postsynaptic spectrin cytoskeleton, with which Ten-m colocalized (Fig. 1e). Postsynaptic α-spectrin normally surrounds the bouton (Fig. 3e). Perturbing neuronal or muscle Teneurins markedly reduced postsynaptic α-spectrin without affecting Dlg (Fig. 3f–h, S7). Postsynaptic β-spectrin[21], Adducin[22] and Wsp were similarly affected (Fig. S8). In the muscle, α-spectrin is coincident with and essential for the integrity of the membranous subsynaptic reticulum (SSR)[21,23]. Consistent with this, *teneurin* disruption reduced SSR width up to 70% (Fig. S9d–g) and increased the frequency of "ghost" boutons, which are failures of postsynaptic membrane organization[23] (Fig. S9a–d). Thus, Teneurins are involved in the organization of the pre- and postsynaptic cytoskeletons and postsynaptic membranes. Further, endogenous α-spectrin co-immunoprecipitated with muscle-expressed, FLAG-tagged Ten-m (Fig. 3i), suggesting that Ten-m physically links the synaptic membrane to the cytoskeleton.

As the most severe defects following *teneurin* perturbation were cytoskeletal, we propose that Teneurins primarily organize the presynaptic microtubule and postsynaptic spectrin-based cytoskeletons (Fig. 3j), which then organize additional synaptic aspects[20,21]. However, such a solitary role cannot fully explain the observed phenotypes. The bouton number defects associated with cytoskeletal disruption are milder than those following

teneurin disruption[20,21,24]. Also, while active zone dynamics are affected by cytoskeletal perturbation[21], defects in apposition are not[21,25]. Moreover, the T-bar structural defects more closely resemble synapse adhesion and active zone formation defects[17,18]. Thus, Teneurins may regulate release site organization and synaptic adhesion independent of the cytoskeleton (Fig. 3j).

Our data also indicate that Teneurins act bi-directionally across the synaptic cleft. Ten-a acts predominantly neuronally as evidenced by localization, phenotypes caused by neuronal (but not muscle) knockdown, and mutant rescue by neuronal (but not muscle) expression (Fig. 2–3, S2–4, S6–7, S9). Yet, in addition to the presynaptic phenotypes, many others were postsynaptic, including reduced muscle spectrin, SSR and membrane apposition (Fig. 3, S7–9). Similarly, although Ten-m is present both pre-and postsynaptically, muscle knockdown resulted in presynaptic defects, including microtubule and vesicle disorganization, reduced active zone apposition, and T-bar defects (Fig. 2–3, S3–4, S6–7). Thus, Teneurins function in bi-directional transsynaptic signaling to organize neuromuscular synapses. This may involve downstream pathways or simply establish an organizational framework by the receptors themselves. Moreover, as the single disruptions of neuronal *ten-a* or muscle *ten-m* were similarly severe and not enhanced by combination (Fig. 2g, 3d, 3h, S2k), they likely function in the same pathway. Our finding that Ten-a and Ten-m co-immunoprecipitate from different cells *in vitro*[8] and across the NMJ *in vivo* (Fig. 1f) further suggests a signal via trans-synaptic complex. Teneurin function, however, may not be solely transsynaptic. In some cases (vesicle density, SSR width), cell-autonomous knockdown showed stronger phenotypes than knocking down in synaptic partners (Fig. S3, S4, S9, Table S1). This suggests additional cell-autonomous roles unrelated to transsynaptic Teneurin signaling.

Signaling involving the transmembrane proteins Neurexin and Neuroligin also mediates synapse development[26]. In *Drosophila*, Neurexin (*dnrx*) and Neuroligin1 (*dnlg1*) mutations cause phenotypes similar to *teneurin* perturbation: reduced boutons, active zone organization, transmission and SSR[27,28]. *dnlg1* and *dnrx* mutations do not enhance each other, suggesting their function in the same pathway[28]. Consistently[27,28], we found that *dnrx* and *dnlg1* mutants exhibited largely similar phenotypes (not shown). To investigate the relationship between the *teneurins* and *dnrx*/*dnlg1*, we focused on the *dnlg1* null mutant. Both Ten-m and DNlg1-eGFP occupied similar postsynaptic space (Fig. S10a). *teneurin* and *dnlg1* loss-of-function also displayed similar bouton number reductions (Fig. 2e, g), vesicle disorganization (Fig. S4) and ghost bouton frequencies (Fig. S9). Other phenotypes showed notable differences in severity. In *dnlg1* mutants, there was a 29% failure of active zone/ glutamate receptor apposition (Fig. 2k, S10d), compared to 15% for the strongest *teneurin* perturbation. For the cytoskeleton, *dnlg1* mutants were mildly impaired compared to *teneurin* perturbations (Fig. 3d, 3h, S6, S7).

To further examine their interplay, we analyzed *ten-a dnlg1* double mutants. Both single mutants were viable, despite their synaptic defects. Double mutants, however, were larval lethal. We obtained rare escapers, which displayed a 72% reduction in boutons, compared to a 50–55% decrease in single mutants (Fig. 2e). Active zone apposition in double mutants was enhanced synergistically over either single mutant (Fig. 2k, S10e). Cytoskeletal defects in the double mutant resembled the *ten-a* mutant (Fig. 3, S6–7). These data suggest that

teneurins and *dnrx/dnlg1* act in partially overlapping pathways, cooperating to properly organize synapses, with Teneurins contributing more to cytoskeletal organization and Neurexin/Neuroligin to active zone apposition (Fig. 3j).

In the accompanying manuscript[8], we showed that while the basal Teneurins are broadly expressed in the *Drosophila* antennal lobe, elevated expression in select glomeruli mediates olfactory neuron partner matching. At the NMJ, this basal level mediates synapse organization. Analogous to the antennal lobe, we found elevated *ten-m* expression at muscles 3 and 8 using the *ten-m-GAL4* enhancer trap (Fig. 4a). We confirmed this for endogenous *ten-m*, and determined that it was contributed by elevated Ten-m expression in both nerves and muscles (Fig. 4b–g). Indeed, *ten-m*-GAL4 was highly expressed in select motoneurons, including MN3-Ib, which innervates muscle 3[29] (Fig. S11c). This elevated larval expression also varied along the anterior-posterior axis (Fig. S12), and was specific for Ten-m as Ten-a expression did not differ within or between segments (not shown).

To test whether elevated Ten-m expression in muscle 3 and MN3-Ib affects neuromuscular connectivity, we expressed *ten-m* RNAi using *ten-m-GAL4*. Wild-type muscle 3 was almost always innervated (Fig. 4h). However, following *ten-m* knockdown, muscle 3 innervation failed in 11% of hemisegments (Fig. 4i–j). This required Ten-m on both sides of the synapse, as the targeting phenotype persisted following neuronal or muscle RNAi suppression using tissue-specific *GAL80* transgenes (Fig. 4j). *ten-a* RNAi did not show this phenotype (Fig. 4j), consistent with homophilic target selection via Ten-m. The phenotype was specific to muscle 3, as innervation onto the immediately proximal or distal muscle was unchanged (Fig. 4j). The low penetrance is likely due to redundant target selection mechanisms[30]. Where innervation did occur, the terminal displayed similarly severe phenotypes to other NMJs (not shown). Thus, in addition to generally mediating synaptic organization, Ten-m also contributes to correct target selection at a specific NMJ.

To determine whether Ten-m overexpression could alter connectivity, we expressed Ten-m in muscle 6 (but not the adjacent muscle 7), and the motoneurons innervating both muscles using *H94-GAL4*. Normally, 60% of the boutons at muscles 6/7 are present on muscle 6 with 40% on muscle 7 (Fig. 4k,m). Ten-m overexpression caused a shift whereby 81% of boutons synapsed onto muscle 6 and only 19% onto muscle 7 (Fig. 4l–m). This shift also required both neuronal and muscle Ten-m as neuronal or muscle GAL80 abrogated it (Fig. 4m). The effect was specific as Ten-a overexpression did not alter this synaptic balance (Fig. 4m), nor was it secondary to altered bouton number, which is unchanged (not shown). Therefore, elevated Ten-m on both sides of the NMJ can bias target choice. This, combined with evidence that Ten-m can engage homophilic interaction *in vitro*[8], supports a transsynaptic homophilic attraction model at the NMJ as in the olfactory system.

In summary, we identified a two-tier mechanism for Teneurin function in synapse development at the *Drosophila* NMJ. At the basal level, Teneurins are expressed at all synapses and engage in hetero- and homophilic bi-directional transsynaptic signaling to properly organize synapses (Fig. 3j). Supporting this, the Teneurins can mediate homo-and heterophilic interactions *in vitro*[8] and heterophilic interactions *in vivo* (Fig. 1f). At the synapse, Teneurins organize the cytoskeleton, interact with α-spectrin, and enable proper

adhesion and release site formation. Further, elevated Ten-m expression regulates target selection in specific motoneurons and muscles via homophilic matching and functions with additional molecules[30] to mediate precise neuromuscular connectivity. Teneurin-mediated target selection at the NMJ is analogous to its role in olfactory synaptic partner matching[8]. As the Teneurins are expressed broadly throughout the antennal lobe, it remains an attractive possibility that they also regulate central synapse organization.

METHODS SUMMARY

Detailed methods on *Drosophila* stocks, immunostaining, electron microscopy, functional assays, construction of epitope-tagged Teneurin constructs, immunoprecipitation, imaging and statistical analysis can be found in Methods.

METHODS

Drosophila Stocks

All *Drosophila* strains and controls were raised at 29°C to maximize GAL4 expression. All mutants and transgenes were maintained over GFP balancer chromosomes to enable larval selection. *Mhc-GAL4* or *DMef2-GAL4*[31] was used to drive expression in all somatic muscles. *Nrv2-GAL4*[32] and *elav-GAL4*[33] were used to drive expression in all neurons. *H94-GAL4* was used to drive expression in muscles 6, 13 and 4 and their corresponding motoneurons[34]. *Daughterless-GAL4* was used to drive expression ubiquitously[35]. *Synj-QF*[36] was used to drive expression in all nerves. *NP6658-GAL4 (ten-m-GAL4)* was used to drive expression in the pattern of endogenous Ten-m expression[8]. The *Df(X)ten-a* deletion was used as a *ten-a* null mutant[8]. For *dnlg1* mutants, the I960 and ex2.3 alleles were used in *trans*[28] and double mutant larvae with *ten-a* were obtained using optimized rearing conditions[37]. Due to the early lethality of the *ten-m* mutant[11], and to independently assess *ten-a*, tissue-specific RNAi was utilized to assess *teneurin* perturbation using the following interfering RNA (IR) transgenic strains: for *ten-m*, UAS-*ten-m*$^{RNAi-V51173}$ and for *ten-a*[8], *UAS-ten-a*$^{RNAi-V32482}$. The following transgenic strains were used: *UAS-Dcr2*[38], *UAS-FasII*[34], *UAS-mCD8GFP*[39], *UAS-DNlg1-eGFP*[28], *UAS-Ten-a*[8], *P[GS]9267* for *ten-m* overexpression[8]. In all cases, the efficacy of interfering RNA (IR, RNAi) transgenes, overexpression transgenes and the *ten-a* deletion mutant were assessed and verified by the alteration of antibody staining (loss, reduction or increase) using tissue-specific *GAL4* drivers. For all cases, N-IR indicates neuronal RNAi, M-IR indicates muscle RNAi, U-IR indicates ubiquitous RNAi. For rescuing *ten-a* mutants, Ten-a N indicates neuronal overexpression with *elav-GAL4* of *UAS-ten-a* and Ten-a M indicates muscle overexpression of *UAS-ten-a* with *DMef2-GAL4*.

Immunostaining

Wandering third instar larvae were processed as previously described[23]. The following primary antibodies were used: mouse antibody to Ten-m (mAb20, 1:500)[40], guinea pig antibody to Ten-a (1:100)[41], mouse antibody to Brp (mAbnc82, 1:250)[42], rabbit antibody to Synaptotagmin I (1:4000)[43], mouse antibody to Cysteine String Protein (mAb6D6, 1:100)[44], mouse antibody to Dlg (mAb4F3, 1:500)[45], rabbit antibody to Dlg (1:40000)[46], mouse

antibody to α-spectrin (mAb3A9, 1:50)[47], mouse antibody to Fasciclin II (mAb1D4, 1:20)[48], rabbit antibody to Fasciclin II (1:5000)[46], mouse antibody to Futsch (mAb22C10, 1:50)[20], rabbit antibody to DGluRIII (1:2500)[15], rat antibody to Elav (mAb7E8A10, 1:25)[49], mouse antibody to Even-skipped (mAb3C10, 1:100)[50], rabbit antibody to β-spectrin (1:1000)[51], mouse antibody to Hts (1:500)[22], guinea pig antibody to Wsp (1:1000)[52]. Alexa488-, Alexa546-, or Alexa647-conjugated secondary antibodies were used at 1:250 (Invitrogen). Texas Red-conjugated Phalloidin was used at 1:300 FITC-, Cy3-, or Cy5-conjugated antibodies to horseradish peroxidase were used at 1:100 (Jackson ImmunoResearch).

Electron Microscopy

Wandering third instar larvae were processed and sectioned as described[23]. Sections were imaged on a JEM-1400 (JEOL) transmission electron microscope at 3000X to 20000X magnification.

Electrophysiology

Larvae were dissected in HL3 saline[53] containing 0 mM Ca^{2+} and 4 mM Mg^{2+}. They were then transferred to saline containing 0.6 mM Ca^{2+} and recordings conducted by impaling larval muscle 6 in body wall segments A3 and A4 using sharp intracellular electrodes (10–20 MΩ), fabricated from borosilicate glass capillaries and filled with 3 M KCl solution. For evoked EPSPs, severed nerve bundles were stimulated using a suction electrode connected to a linear stimulus isolated (A395, World Precision Instruments). Data, acquired using Multiclamp 700B amplifiers (Molecular Devices), was low-pass filtered at 3 kHz and digitized at 10 kHz. Recordings were acquired and analyzed using Igor Pro software (Wavemetrics) and custom-written programs. All recordings in which the resting membrane potential was > -60 mV and/or whose resting potential, input resistance or access resistance changed by more than 20% during the duration of data acquisition were excluded from analysis. All recordings and data analyses were performed blind to the genotype. Quantal content was corrected for nonlinear summation[54].

Larval Locomotion

Crawling assays were conducted as described[55].

FM1-43 Dye Loading

FM1-43 (Invitrogen) dye loading was conducted as described[56] with the following modifications: loading was conducted in 1.5 mM Ca^{2+}, 90 mM K^+ saline for 1 minute followed by six 2-minute washes in 0 mM Ca^{2+} saline. Imaging was conducted on a Zeiss LSM 510 Meta Confocal (Carl Zeiss) with a 40X, PlanApo NA 1.0 water immersion lens (Carl Zeiss).

Construction of Epitope-tagged Teneurin Transgenes—The *ten-m* and *ten-a* coding sequences lacking the stop codon were cloned into *pENTR-D/TOPO* (Invitrogen) from *pENTR-ten-m* and *pENTR-ten-a*[8]. *pENTR-ten-m(-stop)* and *pENTR-ten-a(-stop)* were recombined into the destination vectors *pUASTattB-gtw-tFHAH* and *pQUASTattB-gtw-*

tFMH, respectively, using LR Clonase II (Invitrogen). pUASTattB-gtw-tFHAH is a pUASt-Gateway-attB based vector with a C-terminal TEV recognition site and 3xFLAG, 3xHA and 10xHis tags. *pQUASTattB-gtw-tFMH* is a *pQUASt-Gateway-attB*[8] based vector with a C-terminal TEV recognition site and 3xFLAG, 6xMyc and 10xHis tags. The resulting constructs were verified by restriction digest and sequencing and integrated into the *attP24* or *86Fb* landing sites on the second and third chromosomes[57]. Transgenic flies were verified by IP on Western blot and overexpression experiments.

Immunoprecipitation, Western blots and SDS-PAGE Analysis

For Ten-m and Ten-a, *QUAS-Ten-a-FLAG-Myc* was expressed in nerves using *Synj-QF* and *UAS-Ten-m-FLAG-HA* in muscles using *Mhc-GAL4*. Larval synaptosomes were prepared from larval body wall fillets as described[58]. For Ten-m and α-spectrin, control larvae consisted of *DMef2-GAL4* without *UAS-Ten-m-FLAG-HA* while experimental flies combined the two. Immunoprecipitation was conducted as described using M2-anti-FLAG-conjugated agarose (Sigma) or Affi-Prep Protein A beads (Bio-Rad) and rat antibodies to HA (Roche)[23]. Proteins were separated on NuPAGE 3 – 8% Tris-Acetate Gels (Invitrogen) and transferred to nitrocellulose. Primary antibodies were applied overnight at 4°C and secondary antibodies at 21°C for 1 hour. The following primary antibodies were used: mouse antibody to α-spectrin (mAb3A9, 1:2000), mouse antibody to Brp (mAbnc82, 1:100), mouse antibody to FLAG (M2, 1:5000, Sigma-Aldrich), mouse antibody to Myc (3E10, 1:1500, Santa Cruz Biotechnology), rat antibody to HA (3F10, 1:1500, Roche). HRP-conjugated secondary antibodies (Jackson ImmunoResearch) were used at 1:10000. Blots were developed using the SuperSignal West Femto Maximum Sensitivity Substrate (ThermoScientific).

Imaging Analysis

Larvae were imaged with a Zeiss LSM 510 Meta laser-scanning confocal microscope (Carl Zeiss) using either a 63X 1.4 NA or a 40X 1.0 NA objective. NMJ images were taken as confocal z-stacks with the upper and lower bounds defined by HRP staining unless otherwise noted. For all metrics, boutons were assessed in segment A3 at muscle 6/7 and muscle 4 on both the left and right sides. Fluorescence intensity measurements were taken from terminals on muscle 4. All phenotypes, however, were observed at all synapses regardless of muscle fiber or segment. For membrane organization and Teneurin colocalization, NMJ images were taken as single optical sections at the precise center of the bouton as determined by HRP staining. Images were processed with the LSM software and Adobe Photoshop CS4. Bouton number, active zone / glutamate receptor apposition, fluorescent intensity and microtubule organization were quantified as previously described[23]. Targeting errors for each larva were quantified as the percentage of hemisegments from A1 to A7 in a single animal with a failure of target innervation. There was no difference in targeting errors based on body wall segment. Experiments using H94-GAL4 were conducted as described[34], and their effects confirmed using Fasciclin II overexpression (Control = 58.1% of boutons on muscle 6, 41.9% on muscle 7; Fas II overexpression = 73.0% on muscle 6, 27.0% on muscle 7; n = 8 animals for each, p < 0.0001)[34].

In electron micrographs, parameters were quantified as previously described using ImageJ (National Institutes of Health)[23]. T-bar defects were classified into one of five categories: Normal (no discernible defect), Double (two T-bars were observed in the same, continuous active zone), Detached (where the T-bar was clearly visible but was not explicitly connected to the membrane associated with the nearest PSD), Apposite Contractile Tissue (where the T-bar was not apposed to the SSR, but rather, the contractile tissue of the muscle), Misshapen (where an electron-dense T-bar was visible but did not conform to the "T" shape. Often, the T-bars were "X" shaped). For Fig. 2r, each defect is expressed as a percentage of the total number of T-bars observed in a particular genotype.

For Ten-m gradient calculation, single optical sections were taken through the center of the NMJ on muscle 3 or muscle 4, as determined by HRP immunoreactivity. The GFP signal (*ten-m-GAL4*) or antibody signal was then measured using ImageJ (National Institutes of Health). For each larva, measurements were taken on the right and left sides of each indicated segment. The fluorescence for each segment was expressed as a percentage of the fluorescence from segment A1 in the same animal, on the same side of the larvae. For all larvae, segment A1 represented the maximal fluorescence.

Statistical Analysis

Statistical analysis used GraphPad Prism 5 (Graphpad Software). In all cases involving more than two samples, significance was calculated using ANOVA followed by a Dunnett *post-hoc* test to the control sample and a Bonferroni *post-hoc* test among all samples. For two-sample cases, an unpaired student's *t*-test was used to assess significance, unless otherwise indicated. In all cases, both methods provided similar significance measurements. In all figures, significance is with respect to control genotypes unless otherwise noted.

Supplementary Material

Refer to Web version on PubMed Central for supplementary material.

Acknowledgments

References

1. Williams ME, de Wit J, Ghosh A. Molecular mechanisms of synaptic specificity in developing neural circuits. Neuron. 2010; 68:9–18. [PubMed: 20920787]

2. Giagtzoglou N, Ly CV, Bellen HJ. Cell adhesion, the backbone of the synapse: "vertebrate" and "invertebrate" perspectives. Cold Spring Harb Perspect Biol. 2009; 1:a003079. [PubMed: 20066100]

3. Young TR, Leamey CA. Teneurins: important regulators of neural circuitry. Int J Biochem Cell Biol. 2009; 41:990–993. [PubMed: 18723111]

4. Kenzelmann D, Chiquet-Ehrismann R, Leachman NT, Tucker RP. Teneurin-1 is expressed in interconnected regions of the developing brain and is processed in vivo. BMC Dev Biol. 2008; 8:30. [PubMed: 18366734]

5. Li H, Bishop KM, O'Leary DD. Potential target genes of EMX2 include Odz/Ten-M and other gene families with implications for cortical patterning. Mol Cell Neurosci. 2006; 33:136–149. [PubMed: 16919471]

6. Silva JP, et al. Latrophilin 1 and its endogenous ligand Lasso/teneurin-2 form a high-affinity transsynaptic receptor pair with signaling capabilities. Proc Natl Acad Sci U S A. 2011; 108:12113–12118. [PubMed: 21724987]

7. Leamey CA, et al. Ten_m3 regulates eye-specific patterning in the mammalian visual pathway and is required for binocular vision. PLoS Biol. 2007; 5:e241. [PubMed: 17803360]

8. Hong W, Mosca TJ, Luo L. Teneurins Instruct Synaptic Partner Matching in an Olfactory Map. Nature. 2012; (This Issue)

9. Liebl FL, et al. Genome-wide P-element screen for Drosophila synaptogenesis mutants. J Neurobiol. 2006; 66:332–347. [PubMed: 16408305]

10. Kurusu M, et al. A screen of cell-surface molecules identifies leucine-rich repeat proteins as key mediators of synaptic target selection. Neuron. 2008; 59:972–985. [PubMed: 18817735]

11. Zheng L, et al. Drosophila Ten-m and Filamin Affect Motor Neuron Growth Cone Guidance. PLoS One. 2011; 6:e22956. [PubMed: 21857973]

12. Sone M, et al. Synaptic development is controlled in the periactive zones of Drosophila synapses. Development. 2000; 127:4157–4168. [PubMed: 10976048]

13. Wagh DA, et al. Bruchpilot, a Protein with Homology to ELKS/CAST, Is Required for Structural Integrity and Function of Synaptic Active Zones in Drosophila. Neuron. 2006; 49:833–844. [PubMed: 16543132]

14. Potter CJ, Tasic B, Russler EV, Liang L, Luo L. The Q system: a repressible binary system for transgene expression, lineage tracing, and mosaic analysis. Cell. 2010; 141:536–548. [PubMed: 20434990]

15. Marrus SB, Portman SL, Allen MJ, Moffat KG, DiAntonio A. Differential localization of glutamate receptor subunits at the Drosophila neuromuscular junction. J Neurosci. 2004; 24:1406–1415. [PubMed: 14960613]

16. Wichmann C, Sigrist SJ. The active zone T-bar--a plasticity module? J Neurogenet. 2010; 24:133–145. [PubMed: 20553221]

17. Aberle H, et al. wishful thinking encodes a BMP type II receptor that regulates synaptic growth in Drosophila. Neuron. 2002; 33:545–558. [PubMed: 11856529]

18. Owald D, et al. A Syd-1 homologue regulates pre- and postsynaptic maturation in Drosophila. J Cell Biol. 2010; 188:565–579. [PubMed: 20176924]

19. Kittel RJ, et al. Bruchpilot promotes active zone assembly, Ca2+ channel clustering, and vesicle release. Science. 2006; 312:1051–1054. [PubMed: 16614170]

20. Roos J, Hummel T, Ng N, Klambt C, Davis GW. Drosophila Futsch regulates synaptic microtubule organization and is necessary for synaptic growth. Neuron. 2000; 26:371–382. [PubMed: 10839356]

21. Pielage J, Fetter RD, Davis GW. A postsynaptic spectrin scaffold defines active zone size, spacing, and efficacy at the Drosophila neuromuscular junction. J Cell Biol. 2006; 175:491–503. [PubMed: 17088429]

22. Pielage J, Bulat V, Zuchero JB, Fetter RD, Davis GW. Hts/Adducin controls synaptic elaboration and elimination. Neuron. 2011; 69:1114–1131. [PubMed: 21435557]

23. Mosca TJ, Schwarz TL. The nuclear import of Frizzled2-C by Importins-beta11 and alpha2 promotes postsynaptic development. Nat Neurosci. 2010; 13:935–943. [PubMed: 20601947]

24. Featherstone DE, Davis WS, Dubreuil RR, Broadie K. Drosophila alpha- and beta-spectrin mutations disrupt presynaptic neurotransmitter release. J Neurosci. 2001; 21:4215–4224. [PubMed: 11404407]

25. Miech C, Pauer HU, He X, Schwarz TL. Presynaptic local signaling by a canonical wingless pathway regulates development of the Drosophila neuromuscular junction. J Neurosci. 2008; 28:10875–10884. [PubMed: 18945895]

26. Craig AM, Kang Y. Neurexin-neuroligin signaling in synapse development. Curr Opin Neurobiol. 2007; 17:43–52. [PubMed: 17275284]

27. Li J, Ashley J, Budnik V, Bhat MA. Crucial role of Drosophila neurexin in proper active zone apposition to postsynaptic densities, synaptic growth, and synaptic transmission. Neuron. 2007; 55:741–755. [PubMed: 17785181]

28. Banovic D, et al. Drosophila neuroligin 1 promotes growth and postsynaptic differentiation at glutamatergic neuromuscular junctions. Neuron. 2010; 66:724–738. [PubMed: 20547130]

29. Landgraf M, Roy S, Prokop A, VijayRaghavan K, Bate M. even-skipped determines the dorsal growth of motor axons in Drosophila. Neuron. 1999; 22:43–52. [PubMed: 10027288]

30. Sanes JR, Yamagata M. Many paths to synaptic specificity. Annu Rev Cell Dev Biol. 2009; 25:161–195. [PubMed: 19575668]

31. Lilly B, et al. Requirement of MADS domain transcription factor D-MEF2 for muscle formation in Drosophila. Science (New York, NY. 1995; 267:688–693.

32. Sun B, Xu P, Salvaterra PM. Dynamic visualization of nervous system in live Drosophila. Proc Natl Acad Sci U S A. 1999; 96:10438–10443. [PubMed: 10468627]

33. Luo L, Liao YJ, Jan LY, Jan YN. Distinct morphogenetic functions of similar small GTPases: Drosophila Drac1 is involved in axonal outgrowth and myoblast fusion. Genes Dev. 1994; 8:1787–1802. [PubMed: 7958857]

34. Davis GW, Goodman CS. Synapse-specific control of synaptic efficacy at the terminals of a single neuron. Nature. 1998; 392:82–86. [PubMed: 9510251]

35. Wodarz A, Hinz U, Engelbert M, Knust E. Expression of crumbs confers apical character on plasma membrane domains of ectodermal epithelia of Drosophila. Cell. 1995; 82:67–76. [PubMed: 7606787]

36. Petersen LK, Stowers RS. A Gateway MultiSite Recombination Cloning Toolkit. PLoS One. 2011; 6:e24531. [PubMed: 21931740]

37. Loewen CA, Mackler JM, Reist NE. Drosophila synaptotagmin I null mutants survive to early adulthood. Genesis. 2001; 31:30–36. [PubMed: 11668675]

38. Dietzl G, et al. A genome-wide transgenic RNAi library for conditional gene inactivation in Drosophila. Nature. 2007; 448:151–156. [PubMed: 17625558]

39. Lee T, Luo L. Mosaic analysis with a repressible cell marker for studies of gene function in neuronal morphogenesis. Neuron. 1999; 22:451–461. [PubMed: 10197526]

40. Levine A, et al. Odd Oz: a novel Drosophila pair rule gene. Cell. 1994; 77:587–598. [PubMed: 7514504]

41. Rakovitsky N, et al. Drosophila Ten-a is a maternal pair-rule and patterning gene. Mech Dev. 2007; 124:911–924. [PubMed: 17890064]

42. Laissue PP, et al. Three-dimensional reconstruction of the antennal lobe in Drosophila melanogaster. J Comp Neurol. 1999; 405:543–552. [PubMed: 10098944]

43. Mackler JM, Drummond JA, Loewen CA, Robinson IM, Reist NE. The C(2)B Ca(2+)-binding motif of synaptotagmin is required for synaptic transmission in vivo. Nature. 2002; 418:340–344. [PubMed: 12110842]

44. Zinsmaier KE, Eberle KK, Buchner E, Walter N, Benzer S. Paralysis and early death in cysteine string protein mutants of Drosophila. Science. 1994; 263:977–980. [PubMed: 8310297]

45. Parnas D, Haghighi AP, Fetter RD, Kim SW, Goodman CS. Regulation of postsynaptic structure and protein localization by the Rho-type guanine nucleotide exchange factor dPix. Neuron. 2001; 32:415–424. [PubMed: 11709153]

46. Koh YH, Popova E, Thomas U, Griffith LC, Budnik V. Regulation of DLG localization at synapses by CaMKII-dependent phosphorylation. Cell. 1999; 98:353–363. [PubMed: 10458610]

47. Byers TJ, Dubreuil R, Branton D, Kiehart DP, Goldstein LS. Drosophila spectrin. II. Conserved features of the alpha-subunit are revealed by analysis of cDNA clones and fusion proteins. J Cell Biol. 1987; 105:2103–2110. [PubMed: 2824526]

48. Vactor DV, Sink H, Fambrough D, Tsoo R, Goodman CS. Genes that control neuromuscular specificity in Drosophila. Cell. 1993; 73:1137–1153. [PubMed: 8513498]

49. O'Neill EM, Rebay I, Tjian R, Rubin GM. The activities of two Ets-related transcription factors required for Drosophila eye development are modulated by the Ras/MAPK pathway. Cell. 1994; 78:137–147. [PubMed: 8033205]

50. Patel NH, Schafer B, Goodman CS, Holmgren R. The role of segment polarity genes during Drosophila neurogenesis. Genes Dev. 1989; 3:890–904. [PubMed: 2501154]

51. Byers TJ, Husain-Chishti A, Dubreuil RR, Branton D, Goldstein LS. Sequence similarity of the amino-terminal domain of Drosophila beta spectrin to alpha actinin and dystrophin. J Cell Biol. 1989; 109:1633–1641. [PubMed: 2677025]

52. Ben-Yaacov S, Le Borgne R, Abramson I, Schweisguth F, Schejter ED. Wasp, the Drosophila Wiskott-Aldrich syndrome gene homologue, is required for cell fate decisions mediated by Notch signaling. J Cell Biol. 2001; 152:1–13. [PubMed: 11149916]

53. Stewart BA, Atwood HL, Renger JJ, Wang J, Wu CF. Improved stability of Drosophila larval neuromuscular preparations in haemolymph-like physiological solutions. J Comp Physiol A. 1994; 175:179–191. [PubMed: 8071894]

54. Martin AR. A further study of the statistical composition on the end-plate potential. J Physiol. 1955; 130:114–122. [PubMed: 13278890]

55. Lnenicka GA, Spencer GM, Keshishian H. Effect of reduced impulse activity on the development of identified motor terminals in Drosophila larvae. J Neurobiol. 2003; 54:337–345. [PubMed: 12500309]

56. Verstreken P, Ohyama T, Bellen HJ. FM 1-43 labeling of synaptic vesicle pools at the Drosophila neuromuscular junction. Methods Mol Biol. 2008; 440:349–369. [PubMed: 18369958]

57. Markstein M, Pitsouli C, Villalta C, Celniker SE, Perrimon N. Exploiting position effects and the gypsy retrovirus insulator to engineer precisely expressed transgenes. Nat Genet. 2008; 40:476–483. [PubMed: 18311141]

58. Higashi-Kovtun ME, Mosca TJ, Dickman DK, Meinertzhagen IA, Schwarz TL. Importin-beta11 regulates synaptic phosphorylated mothers against decapentaplegic, and thereby influences synaptic development and function at the Drosophila neuromuscular junction. J Neurosci. 2010; 30:5253–5268. [PubMed: 20392948]
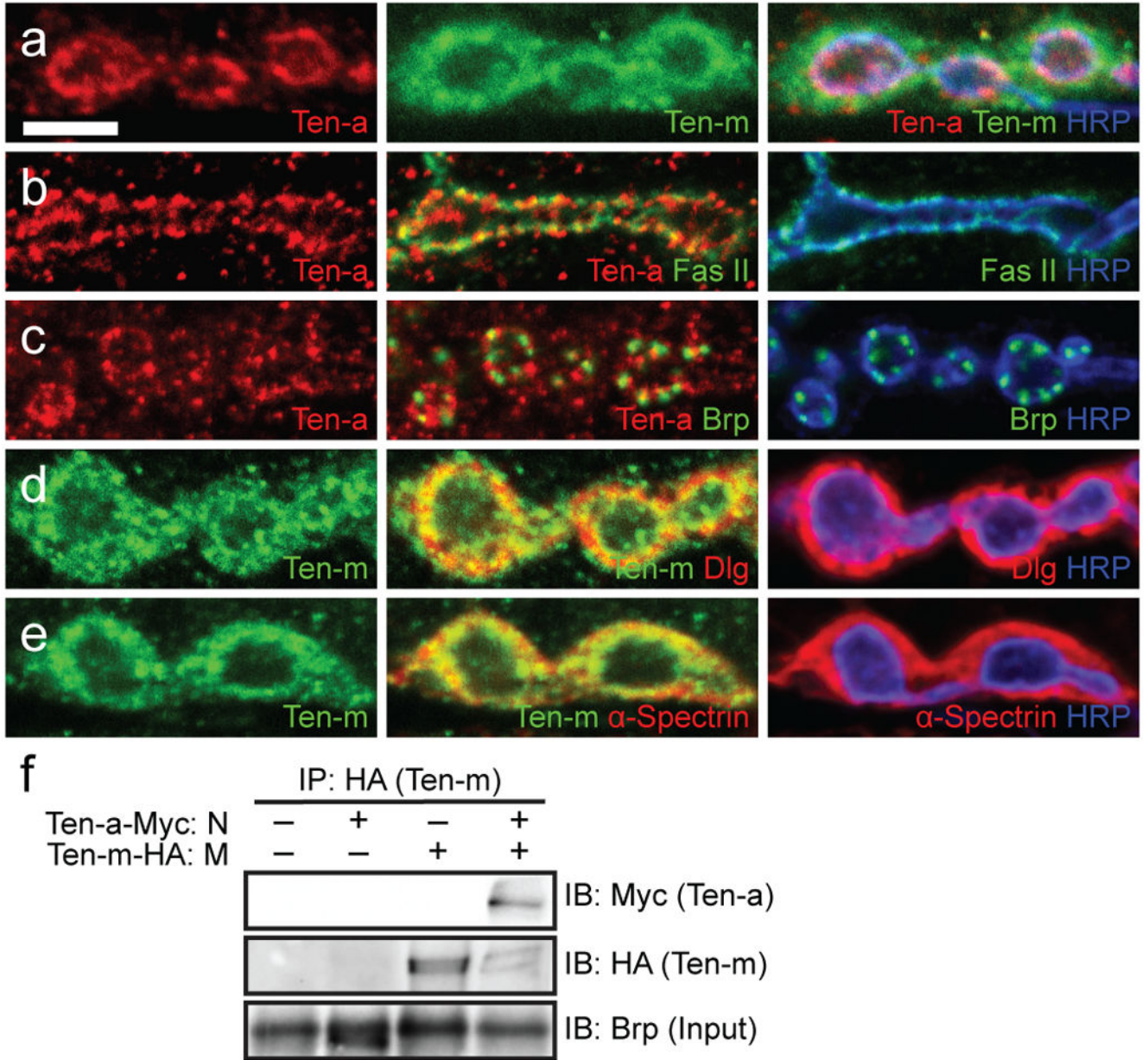
Figure 1. Teneurins are Enriched at and Interact across *Drosophila* Neuromuscular Synapses
a – e, Representative single confocal sections of synaptic boutons stained with antibodies against Ten-a (red) or Ten-m (green), HRP to mark neuronal membrane (blue) and a synaptic marker as indicated. Ten-a is associated with presynaptic membranes and Ten-m largely with the surrounding postsynapse (**a**). Ten-a has limited colocalization with a periactive zone marker Fasciclin II (**b**), and Bruchpilot (Brp), an active zone marker (**c**). Ten-m colocalizes with, and extends beyond, Dlg (**d**) and completely with muscle α-spectrin (**e**). **f**, Immunoblots (IB) of larval synaptosomes expressing neuronal FLAG-Myc-tagged Ten-a (N) and muscle FLAG-HA-tagged Ten-m (M) and immunoprecipitated (IP) using HA antibodies. Ten-a is detected in the pull-down, indicating that nerve Ten-a and muscle Ten-

m interact across the NMJ. This is not seen in control lanes. Due to low expression, neither transgene product is detectable in input lysates, which are enriched in Brp. Scale = 5 μm.
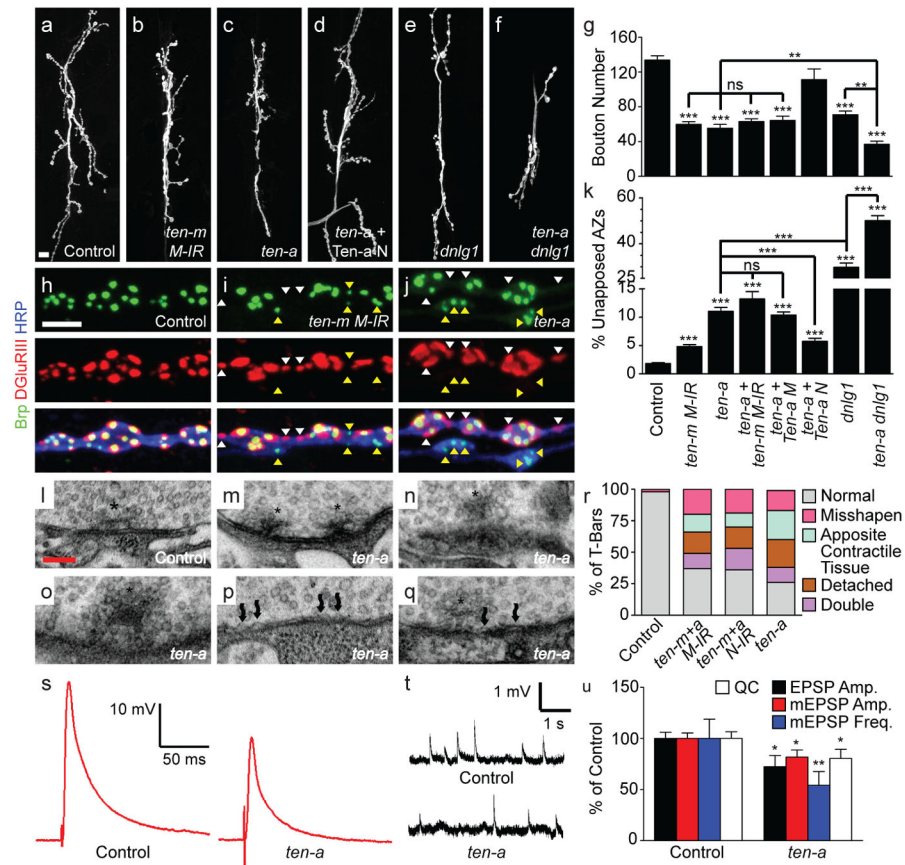
Figure 2. Teneurins Affect Structure and Function of the Neuromuscular Synapse
a – f, Representative NMJs stained with antibodies to HRP. Muscle-specific *ten-m* RNAi
(M-IR) and neuron-specific *ten-a* knockdown (N-IR) decreases bouton number. Neuronal
(Ten-a N) but not muscle (Ten-a M) restoration of *ten-a* expression rescues this phenotype.
These defects resemble *dnlg1* mutants and are enhanced in *ten-a dnlg1* double mutants. **g,**
Quantification of bouton number. **h – j,** Representative NMJs stained with antibodies to Brp
(green), the glutamate receptor DGluRIII (red) and HRP (blue). In control larvae (**h**), Brp
and DGluRIII puncta properly appose. *teneurin* perturbations (**i – j**) disrupt this active zone
(yellow arrowhead) and glutamate receptor apposition (white arrowhead). **k,** Quantification
of unopposed active zone/glutamate receptor pairs. For each quantification, *n* 8 larvae, 16
NMJs. **l – q,** Transmission electron microscopy of active zone T-bars (asterisks) in control
larvae (**l**) and *ten-a* mutants (**m–q**) showing double T-bars (**m**), detached T-bars (**n**),
misshapen T-bars (**o**), membrane ruffling (**p**, waved arrows) and T-bars facing contractile
tissue (**q**). Some images show multiple defects. **r,** Distribution of T-bar defects as a
percentage of the total T-bars. For each genotype, n 3 larvae, 40 boutons. **s – t,**
Representative evoked EPSP (**s**) and mEPSP (**t**) traces from control and *ten-a* mutant
genotypes. **u,** Quantification of mean EPSP amplitude (black), mEPSP amplitude (red),
mEPSP frequency (blue) and quantal content (QC, white) expressed as a percentage of the
control average. For all genotypes, n 7 larvae, 8 muscles. Error bars represent SEM. Scale =
10 μm (**a – f**), 5 μm (**h – j**), 100 nm (**l – q**). In this and all subsequent figures, error bars

represent SEM; *** $p<0.001$, ** $p<0.01$, * $p<0.05$, ns = not significant. Statistical comparisons are with control unless noted.
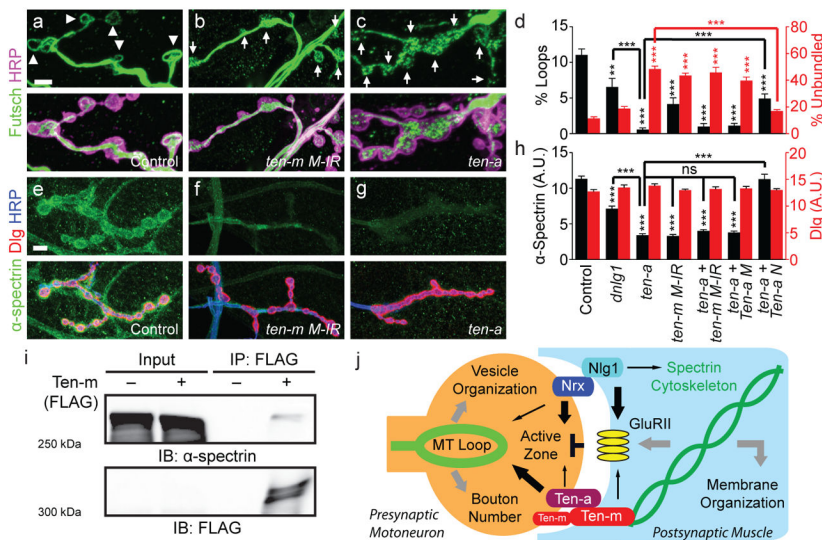
Figure 3. Teneurin Perturbation Results in Marked Cytoskeletal Disorganization
a – c, Representative NMJs stained with antibodies to Futsch (green) and HRP (magenta).
Arrowheads indicate looped organization. Arrows indicate unbundled Futsch. **d**,
Quantification of the percent of total boutons with looped or unbundled microtubules. **e – g**,
Representative NMJs stained with antibodies to α-spectrin (green), Dlg (red) and HRP
(blue). Following *teneurin* perturbation, α-spectrin staining is largely lost. Axonal α-spectrin
is unaffected by muscle *teneurin* RNAi (**f**). **h**, Quantification of α-spectrin (green) and Dlg
(red) fluorescence. For all genotypes, $n \geq 6$ larvae, 12 NMJs. **i**, Immunoblots showing that α-
spectrin is detected in the FLAG-immunoprecipitates of larvae expressing muscle FLAG-
HA-tagged Ten-m but not in control larvae. Due to low expression, FLAG-HA-Ten-m is
only detectable following IP enrichment. **j**, Model showing the roles of Teneurins, Neurexin
and Neuroligin at the NMJ. Arrow size represents the relative contribution of each pathway
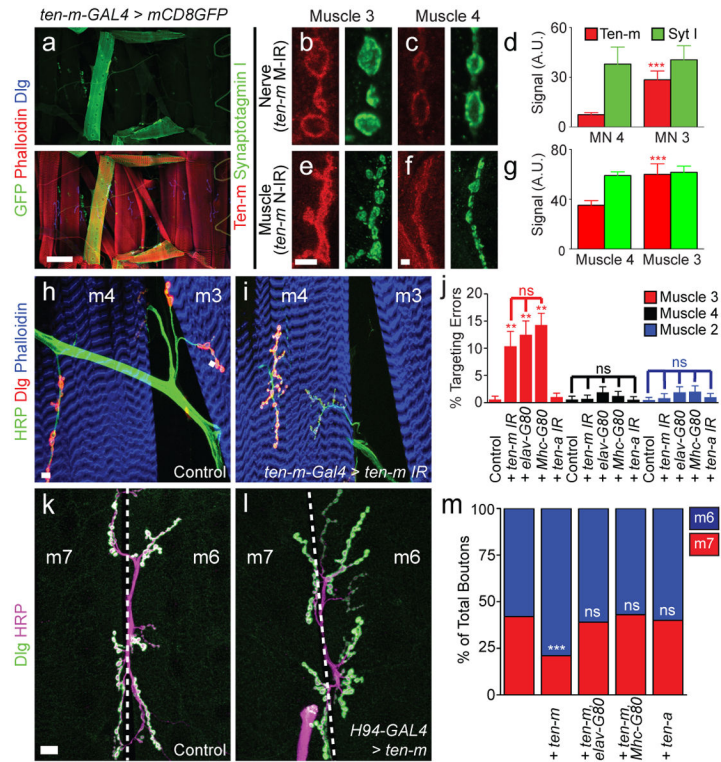to the cellular process as inferred from mutant phenotypic severity. Scale = 5 μm.

Figure 4. High-level Ten-m Expression Regulates Muscle Target Selection

a, Representative images of hemisegment A3 stained with antibodies to Dlg (blue), phalloidin (red) and expressing GFP via *ten-m-GAL4* (green). High-level expression is observed in muscles 3 and 8 and basally in all muscles. **b – c,** Muscle 3 (**b**) and 4 (**c**) NMJs show differential Ten-m (red) but similar Syt I (green) expression (from a *ten-m* muscle knockdown animal). **d**, Quantification of presynaptic Ten-m (red) and Syt I (green) fluorescence at muscle 3 and 4 NMJs. **e – f**, NMJs at muscles 3 (**e**) and 4 (**f**) show differential Ten-m (red) but similar Syt I (green) expression in muscles (from a *ten-m* nerve knockdown). **g**, Quantification of postsynaptic Ten-m (red) and Syt I (green) fluorescence at muscle 3 and 4 NMJs. **h – i**, Representative images stained with phalloidin (blue) and antibodies to HRP (green) and Dlg (red) to visualize motoneurons and muscles in control (**h**) or *ten-m-GAL4>ten-m* RNAi larvae (**i**). **j**, Quantification of the hemisegment percentage with failed muscle 3 (red), 4 (black) or 2 (blue) innervation. **k – l,** Representative images of the muscle 6/7 NMJ labeled with antibodies to Dlg (green) and HRP (magenta). The characteristic wild-type arrangement of boutons (**k**) is shifted toward muscle 6 when Ten-m is overexpressed in that muscle and the innervating motoneurons (**l**). **m**, Quantification of the total bouton percentage on muscles 6 (blue) and 7 (red). All genotypes contain *H94-GAL4*, additional transgenes are indicated. The Ten-m-mediated shift is abolished by neuronal or muscle *GAL80* transgenes. Scale = 100 μm (**a**), 5 μm (**b – i**), 10 μm (**k – l**). In all cases, *n* 12 larvae.